Oxygen isotope systematics of magnetite in hydrated Antarctic micrometeorites: new water reservoir

Elena Dobrica, R C Ogliore, Cecile Engrand, K Nagashima, A. J. Brearley

OXYGEN ISOTOPE SYSTEMATICS OF MAGNETITE IN HYDRATED ANTARCTIC MICROMETEORITES: NEW WATER RESERVOIR. E. Dobrica[1], R. C. Ogliore[2], C. Engrand[3], K. Nagashima[4] and A. J. Brearley[1], [1]Department of Earth and Planetary Sciences MSC03-2040, 1 University of New Mexico, Albuquerque, NM 87131-0001 (edobrica@unm.edu), USA; [2]Department of Physics, Washington University in St. Louis, St. Louis, MO 63117, USA; [3]CSNSM, Univ. Paris Sud, Université Paris-Saclay, 91405 Orsay Campus, France; [4]Hawai‘i Institute of Geophysics and Planetology, University of Hawai‘i at Manoa, Honolulu, HI 96822, USA.

Introduction: Secondary phases in hydrated Antarctic micrometeorites (AMMs) will show an oxygen isotopic signature from their likely formation by aqueous processes, in either a comet or asteroid parent body. Asteroidal water may be distinguishable from cometary water in its oxygen isotopic composition. The oxygen isotopic composition of water in asteroidal-derived hydrated AMMs should be close to $\Delta^{17}O \sim 0$ if their parent body is carbonaceous chondrite (CC)-like (similar to the hydrated interplanetary dust particles (IDPs) measured so far [1]) or $\Delta^{17}O \sim +6.6‰$ if their parent body is ordinary chondrite (OC)-like [e.g. 2-4]. Any hydrated AMMs with significantly different $\Delta^{17}O$ values would be evidence that these particles formed from non-asteroidal water. If Jupiter-family comets (JFCs) accreted outer nebular water, the O composition of their secondary minerals could be similar to the cosmic symplectites (COSs) from Acfer 094 [5-6].

Here we present the mineralogy and oxygen isotope compositions of magnetite grains and a magnetite-dolomite assemblage that were identified in five AMMs. The purpose of these measurements is to investigate the diversity of the water reservoir from which hydrated AMMs formed and the temperature at which these minerals co-precipitated.

Methods: Secondary ion mass spectrometer (SIMS) analyses was carried out using the Cameca ims-1280 ion microprobe. We used a ~25 pA Cs^+ primary beam focused to ~2 µm with total impact energy of 20 keV. Masses $^{16}O^-$, $^{17}O^-$, and $^{18}O^-$ were measured simultaneously in multicollection mode on a Faraday cup and two electron multipliers, respectively. We made sure we cleanly measured the desired phase by later imaging of the analyzed grains by scanning electron microscopy (SEM). We corrected ^{16}OH interference contribution onto ^{17}O (< 0.5‰).

Detailed SEM studies were performed on five polished sections using a FEI Quanta 3D field emission gun (FEG) SEM/FIB operating at 30 kV. Eight transmission electron microscopy (TEM) sections of a selected region containing magnetite with different morphologies were prepared using the FIB technique with a FEI Quanta 3D Dualbeam® FIB. Bright and dark-field TEM images and quantitative EDS X-ray analyses were carried out at 200 kV on a JEOL 2010F FEG TEM/Scanning TEM (STEM).

Results: Five unmelted AMMs (99-12-45, 94-4B-21, 03-26-59, 03-36-46, and 07-13-01, Fig. 1) were analyzed in this study. The first 2 samples were collected from blue ice fields at Cap-Prudhomme [7] and the last 3 from the pristine CONCORDIA snow in 2002 and 2006 [8]. Sample 07-13-01 is a fragment of a larger micrometeorite. The rest are whole particles collected from ice or snow. The AMMs vary in size from 25 x 50 µm (particle 07-13-01) to 100 x 200 µm (particle 94-4B-21).

SEM imaging of the five polished sections analyzed in this study show the presence of magnetite embedded in a fine-grained, fibrous material. An enstatite (En_{88}) of ~15 µm in length was identified in the sample 07-13-01 (Fig. 1d). Magnetite was identified in all particles and has four different morphologies (plaquettes, framboidal, spherulite, anhedral) up to 7 µm in size (Fig. 2). Additionally, we identified a magnetite-dolomite assemblage in 03-36-46 (Fig. 1f).

The TEM study show that the magnetite is associated to phyllosilicates in three of the samples analyzed, except 07-13-01. Sample 07-13-01 was heated during the atmospheric entry as evidenced by the presence of vesicles, which are commonly formed upon melt devolatilization during atmospheric entry. Other signs of heating during the atmospheric entry are observed in the sample 94-4B-21, which shows the presence of a continuous <1 µm-thick magnetite rim (made during atmospheric entry) in one of the FIB sections.

The $\Delta^{17}O$ values of magnetites in the AMMs range from 1.3‰ to 4.2‰ (Fig. 3). The magnetite $\delta^{18}O$ values span a range of ~30‰, much larger than those of analytical artifact [9]. Generally, the magnetites measured show a large range within individual AMMs. For example, the magnetite measured in the sample 94-4B-21 spans the largest range in $\delta^{18}O$: -9.8‰ to +17.4‰. We measured the magnetite-dolomite assemblage to be differ by 18+/- 3‰ (2σ) in $\delta^{18}O$.

Discussion: The oxygen isotopic compositions and the morphologies of the magnetites analyzed in this study show that they are formed during precipitation processes from a gel-like phase during aqueous alteration of the planetesimals [10]. Their O isotopic compositions indicate that the water reservoir from which hydrated AMMs formed is intermediary between CCs and OCs, and that the particles were not modified during the atmospheric entry heating [11]. The $\delta^{18}O$ values of magnetites in AMM 94-4B-21 show a ~27‰ mass-dependent spread in a single 100 x 200 µm particle. This spread is 4 times larger than that for $\delta^{18}O$ values of all magnetites measured in the CR chondrite Renazzo [2] that is in turn orders of magnitude larger in size. It has been suggested that the mass-dependent spread in O isotopes measured in CR indicates changes in fluid temperature and/or composition during magnetite formation [2]. The large heterogeneity of the oxygen isotopic composition could indicate that there was a localized control on the fluid composition.

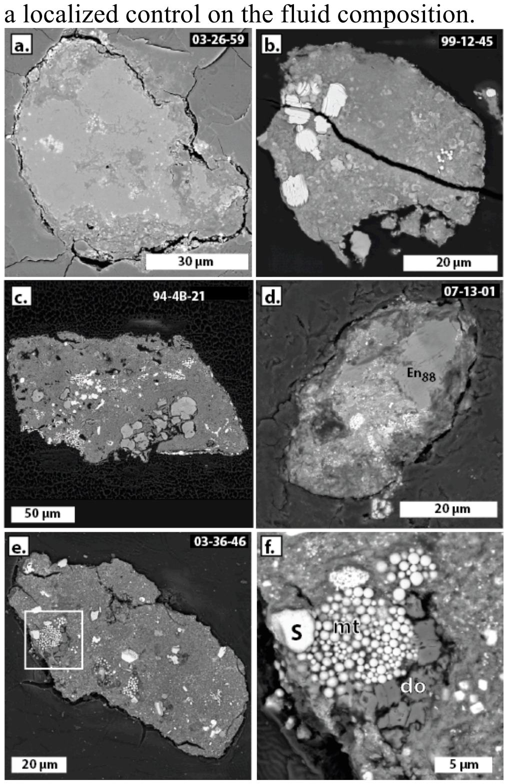

Figure 1. Secondary (a) and backscattered electron (b-f) images showing the AMMs studied. Framboidal magnetite was identified in all five particles. Additionally, plaquettes, spherulite and anhedral magnetite are present in particles 94-4B-21 (c) and 07-13-01 (d). e) Particle 03-36-46 contains a magnetite-dolomite assemblage (details of the white square in 1f). S = sulfide, mt = magnetite, do = dolomite, En = enstatite.

If we assume that the magnetite and dolomite formed in equilibrium, the relative equilibrium O-isotope fractionation between dolomite and magnetite can be used to extract the temperature at which these minerals co-precipitated [e.g. 2]. The $\delta^{18}O$ difference between carbonate and magnetite in the magnetite-dolomite assemblage in 03-36-46 is 18‰, corresponding to the precipitation temperature between 160 and 280°C (100-200°C warmer than a calcite-magnetite assemblage from the CR2 chondrite, Al Rais [2]).

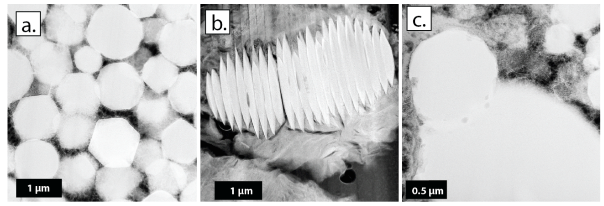

Figure 2. Dark-field STEM images of the different morphologies of magnetites identified in the AMMs studied (a – framboidal, b - plaquettes, and c – anhedral).

Conclusion: Our measurements indicate that the parent-bodies of hydrated AMMs sampled a different water reservoir than the parent bodies of OCs and CCs. Recently, similar results were obtained by the IR and Raman measurements of hydrated AMMs, indicating that the AMMs sampled parent bodies different from CR and CM chondrites [12].

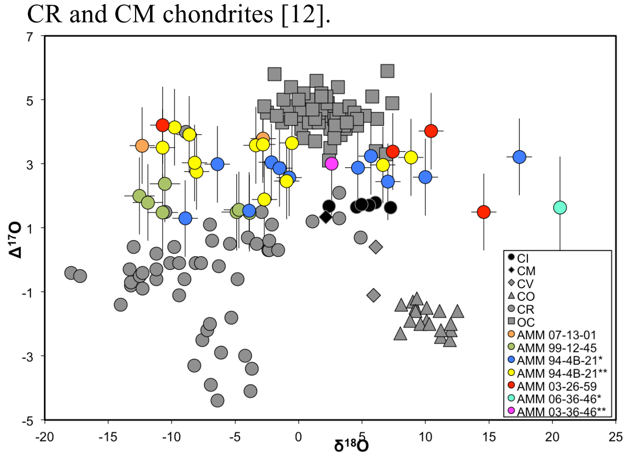

Figure 3. Comparisons between $\Delta^{17}O$ values and $\delta^{18}O$ values of the magnetite from the five AMMs (this work) and one dolomite (03-36-46*, aquamarine circle), OCs (grey squares), and CCs (CO, CR, CV in grey signs [e.g. 2-3] and CM, CI black signs [13]). Framboidal magnetites (*blue circles) measured in the same particle 94-4B-21 have higher average $\delta^{18}O$ (avg. 1.9‰) than the anhedral magnetites (**yellow circles, $\delta^{18}O$ = avg. -3.3‰).

Acknowledgements: This work was funded by NASA grant NNH16ZDA001N to E. Dobrica (PI).

References: [1] Aleon J. et al. (2009) *Geochim. Cosmochim. Acta*, 73:4558-4575. [2] Jilly C. E. et al. (2018) *Geochim. Cosmochim. Acta*, 222:230-252. [3] Doyle P. et al (2015) *Nature Communications* 6:7444. [4] Choi B. G. et al. (1998) *Nature*, 392: 577-579. [5] Sakamoto N. et al. (2007) *Science*, 317:231-233. [6] Seto Y. et al. (2008) *Geochim. Cosmochim. Acta*, 72:2723-2734. [7] Maurette M. et al. (1991) *Nature*, 351:44-47. [8] Duprat J. et al. (2007) *Advance in Space Research* 39:605-611. [9] Huberty J. M. et al. (2010) *Chem. Geol.* 276:269–283. [10] Kerridge J. F. (1979) *Science* 205:395-397. [11] Engrand C. and Dobrica E. (2012) LPSC 43:#2636. [12] Battandier M. et al. (2016) 47th LPSC, #1475. [13] Rowe M. et al (1994) *Geochim. Cosmochim. Acta*, 58:5341-5347.